HHS Public Access

Author manuscript

Neuron. Author manuscript; available in PMC 2022 February 03.

Published in final edited form as:

Neuron. 2021 February 03; 109(3): 461–472.e5. doi:10.1016/j.neuron.2020.11.010.

Area postrema cell types that mediate nausea-associated behaviors

Chuchu Zhang, **Judith A. Kaye**, **Zerong Cai**, **Yandan Wang**, **Sara L. Prescott**, **Stephen D. Liberles**[#]

Howard Hughes Medical Institute, Department of Cell Biology, Harvard Medical School, Boston, MA 02115, USA

SUMMARY

Nausea, the unpleasant sensation of visceral malaise, remains a mysterious process. The area postrema is implicated in some nausea responses, and is anatomically privileged to detect bloodborne signals. To investigate nausea mechanisms, we built an area postrema cell atlas through single-nucleus RNA sequencing, revealing a few neuron types. Using mouse genetic tools for cell-specific manipulation, we discovered excitatory neurons that induce nausea-related behaviors, with one neuron type mediating aversion imposed by multiple poisons. Nausea-associated responses were observed to agonists of identified area postrema receptors, and suppressed by targeted cell ablation and/or gene knockout. Anatomical mapping revealed a distributed network of long-range excitatory but not inhibitory projections with subtype-specific patterning. These studies reveal the basic organization of area postrema nausea circuitry, and provide a framework towards understanding and therapeutically controlling nausea.

Graphical Abstract

[#]Corresponding Author and Lead Contact: Stephen_Liberles@hms.harvard.edu.

AUTHOR CONTRIBUTIONS

CZ and SDL designed the study, analyzed data, and wrote the manuscript; CZ performed all experiments, except ZC performed some two-color expression studies, YW performed dual retrograde AAV injections and prepared custom AAVs, and JAK and SLP assisted with single-nucleus transcriptome analysis.

DECLARATION OF INTERESTS

SDL is a consultant for Kallyope, Inc.

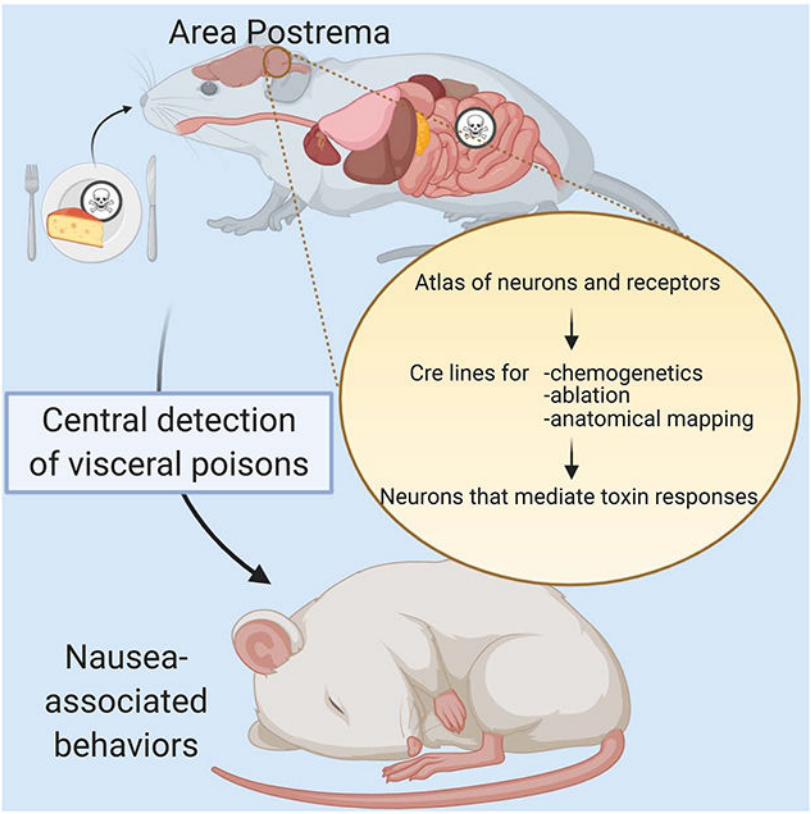

eTOC Blurb

Nausea is an unpleasant sensation of visceral malaise that remains poorly understood at a molecular and cellular level. Here, we use genetic tools based off an area postrema cell atlas to identify neurons and receptors that mediate nausea-related behaviors triggered by visceral poisons.

INTRODUCTION

Nausea is a sickness-associated sensation that has remained almost completely uncharted at a molecular and cellular level. Nausea is frequently associated with vomiting, a forceful evacuation of gastrointestinal contents, and also conditions learned aversion of associated stimuli to avoid future sickness bouts. Many stimuli evoke nausea and/or vomiting, including pathogens, toxins, drug therapies, pregnancy, and motion sickness (Andrews, 1992; Hornby, 2001; Miller and Leslie, 1994). Sickness responses to toxin ingestion and infection are evolutionarily beneficial survival behaviors; however, the sensation of nausea can also be maladaptive, as many treatments for cancer, diabetes, and other illnesses induce nausea as a major adverse side effect. Current anti-nausea medications display highly variable success across patient populations, with nausea being a principal reason why cancer patients are unable to adhere to particular treatment regimens (Hesketh, 2008). Understanding the diversity of molecular and cellular pathways capable of evoking nausea should allow for more effective nausea intervention.

Sensory pathways leading to nausea have remained enigmatic, with several neuronal routes of transmission to the brain possible, including through vagal afferents, area postrema neurons, the vestibular system, and potentially other cell types. The area postrema is a circumventricular organ implicated in nausea and vomiting responses to at least some visceral stimuli (Borison, 1989; Miller and Leslie, 1994; Price et al., 2008). Electrical stimulation of the area postrema evokes nausea and emesis, and lesions of the area postrema eliminate nausea-related responses to particular intravenous toxins, but not to motion sickness (Borison, 1989; Ritter et al., 1980). Mice and other rodents are incapable of vomiting, but some stimuli that evoke nausea and vomiting in humans engage the rodent area postrema and cause robust behavioral aversion to co-presented sensory cues (Andrews, 1992). Additional functions for the area postrema in feeding, metabolism, cardiovascular regulation, and body fluid/cerebrospinal fluid homeostasis have been proposed (Price et al., 2008), with some physiological responses possibly secondary to nausea (Borison, 1989). The area postrema is notably difficult to study, as coarse area postrema lesion or electrical stimulation can potentially impact fibers of passage such as vagal terminals or adjacent brain regions such as the nucleus of the solitary tract (NTS), both of which control many basic autonomic functions (Borison, 1989). Thus, it remains debated whether the area postrema is devoted to processing emetic stimuli, or instead contains diverse cell types involved in distinct physiological functions.

Located at the floor of the fourth ventricle in the brainstem, the area postrema occupies a privileged anatomical location outside the blood-brain barrier (Borison, 1989; Miller and Leslie, 1994; Price et al., 2008). Resident area postrema neurons are uniquely poised to detect bloodborne cues, projecting neurites to the large perivascular spaces of locally fenestrated capillaries. The area postrema is classically considered a brain-resident sensory structure involved in interoception, as it is a key detection site for circulating hydrophilic chemicals that do not readily cross the blood-brain barrier. Several peptides produced peripherally, including glucagon-like peptide 1 (GLP1), amylin, and growth/differentiation factor 15 (GDF15), directly stimulate cohorts of area postrema neurons (Barth et al., 2004; Hsu et al., 2017; Kawatani et al., 2018; Zuger et al., 2013), with GLP1 and amylin responses largely segregated (Zuger et al., 2013). The area postrema also receives second-order inputs from at least some vagal sensory neurons, and top-down inputs from other brain nuclei (Borison, 1989; Miller and Leslie, 1994), and many neurotransmitters activate area postrema neurons (Carpenter et al., 1988; Ferguson and Bains, 1996). These various stimuli can engage divergent cell surface receptors and intracellular signaling pathways involving different second messengers. A systematic analysis of hormone and neurotransmitter receptors present across area postrema neuron types is lacking, as are mechanistic insights into the roles of various area postrema receptors in nausea-associated behaviors.

Here, we used single-nucleus RNA sequencing to investigate area postrema cell diversity, finding that it contains only a few neuron types. Genetic approaches for cell-selective activation, ablation, cAMP imaging, gene knockout, and gene rescue revealed a specific area postrema neuron type that mediates behavioral responses to multiple nausea-inducing stimuli. This cell type expresses a rich assortment of cell surface receptors, and nausea-associated responses to receptor agonists could be predicted and effectively silenced through area postrema-targeted manipulations.

RESULTS

An area postrema cell atlas enables genetic access to neuron subtypes

We investigated cellular diversity in the area postrema using single-nucleus RNA-sequencing (sNuc-seq) (Habib et al., 2016). The area postrema resides outside the blood brain barrier (Figure 1A, S1A) and was acutely harvested using anatomical landmarks to minimize incorporation of adjacent NTS regions (Figure S1B). Nuclei were purified from homogenized tissue on an iodixanol gradient, and isolated in nanoliter sized droplets using an inDrop platform for lysis and barcoded reverse transcription of nuclear RNA. Amplified cDNA was sequenced, and transcriptome data were obtained for 3,678 area postrema cells. Single-cell transcriptome data from area postrema neurons are publicly available (Geo accession number GSE160938).

Unsupervised clustering analysis revealed 1,848 neurons, 1,299 tanycytes, and smaller numbers of other cell types (Figure S1C, S1D). Focused analysis of neuron-derived transcriptomes revealed ten neuronal clusters ranging in size from 75 to 353 neurons (Figure S1E). Six neuronal cell types (clusters 1-4, 8-9) were glutamatergic excitatory neurons together containing 986 neurons, while four cell types (clusters 5-7,10) were GABAergic inhibitory neurons together containing 862 neurons. Signature genes were identified that marked each cluster (Figure 1B, Table S1), and mRNA *in situ* hybridization data from the Allen Brain Atlas (Lein et al., 2007) were analyzed for caudal brainstem expression (Figure S1F). Some signature genes showed expression in both the area postrema and neighboring NTS; at least one signature gene from seven clusters (1-7) was expressed only in the area postrema and not NTS, while three clusters (8-10) contained signature genes expressed in the medial NTS instead of area postrema and are presumably adjacent NTS cell types included in the dissection. We conclude that the area postrema contains four principal excitatory neuron types (clusters 1-4) and three principal inhibitory neuron types (clusters 5-7) (Figure 1C).

Different area postrema neuron types express various cell surface receptors (Figure 1D). GLP1 receptor (*Glp1r*) is expressed in three groups of excitatory neurons (clusters 2, 3, 4), with each cluster also showing enriched expression of genes encoding the noradrenaline transporter (NET), also known as SLC6A2 (cluster 2), angiotensin 2 receptor (cluster 3), or GDF15 receptor GFRAL (cluster 4). A separate group of excitatory neurons (cluster 1) does not express *Glp1r* but instead expresses genes encoding the amylin receptor (CALCR), olfactory receptor 78, and tachykinin receptor 3. We also observed expression of several genes encoding norepinephrine biosynthesis enzymes, including *Th, Ddc, and Dbh* in cluster 2 neurons, but noted sparser expression of the vesicular transporter gene *Slc18a2* (Figure S1G). Area postrema inhibitory neurons also differentially express many cell surface receptor genes, including those encoding ghrelin receptor (cluster 5), gastric inhibitory peptide receptor (cluster 6), and tropomyosin receptor kinase A (clusters 7/6), as well as *Gpr83* and *Tmem215* (Figure S1G). GLP1R-expressing excitatory area postrema neurons express many other genes encoding cell surface receptors whose roles in area postrema neurons are unknown, including the calcium-sensing receptor (CaSR), prolactin-releasing

peptide receptor, GPR88, TRPM3, and TMEM35a. Thus, discrete classes of excitatory and inhibitory area postrema neurons express different repertoires of cell surface receptor genes.

We obtained Cre knock-in mice to gain genetic access to subtypes of area postrema excitatory neurons (Figure 1E). We previously generated *Glp1r-ires-Cre* mice (Williams et al., 2016), obtained *Calcr-ires-Cre* mice (Pan et al., 2018), and now generated *Gfral-p2a-Cre* and *Slc6a2-p2a-Cre* mice. Two-color expression analysis revealed that most receptor-expressing cells produced Cre-dependent reporters (Figure S2); as is common for Cre lines, some receptor-negative reporter-positive cells were also observed, presumably due to receptor expression that was transient or too low for detection by RNA *in situ* hybridization.

Distinct neuron types of the area postrema promote aversion

The area postrema mediates illness responses to certain manifestations of visceral malaise. Here, we used chemogenetic approaches to activate small neuronal clusters within the area postrema and ask whether they condition avoidance to presented flavor cues. Area postrema GLP1R neurons were of particular interest, as GLP1R agonists control insulin release, blood glucose levels, and feeding behavior, and are a clinical mainstay for diabetes treatment (Baggio and Drucker, 2007). However, GLP1R agonists also induce nausea as a side effect and it is unclear whether appetite suppression and nausea involve overlapping neural pathways. *Glp1r* is expressed in neurons of the area postrema, NTS, hypothalamus, and vagus nerve, and a role for area postrema *Glp1r* in nausea and/or satiety is unknown (Adams et al., 2018; Fortin et al., 2020; Yamamoto et al., 2003).

GLP1R and CALCR agonists induce electrical responses and Fos expression in area postrema neurons (Kawatani et al., 2018; Riediger et al., 2001; Zuger et al., 2013), presumably through activating a $G\alpha_s$/cAMP signaling pathway (Lin et al., 1991; Thorens, 1992). Indeed, when area postrema neurons from *Glp1r-ires-Cre; Rosa26-LSL-tdTomato* and *Calcr-ires-Cre; Rosa26-LSL-tdTomato* mice were transfected with the genetically encoded fluorescent cAMP sensor cADDis (Tewson et al., 2016), cAMP responses were observed to the GLP1R agonist exendin-4 in 38% (88/231) of all neurons, 90% (26/29) of GLP1R neurons, and 12% (4/34) of CALCR neurons (Figure 2A, B). Conversely, pramlintide responses were observed in 19% (29/151) of all neurons, 14% (3/21) of GLP1R neurons, and 50% (12/24) of CALCR neurons (Figure 2C). The amylin co-receptor RAMP3 is enriched in area postrema relative to NTS (Figure S1F), so some non-responsive CALCR neurons may be RAMP3-negative NTS neurons included in the analysis. These findings provide further evidence that GLP1R and CALCR area postrema neurons are largely segregated populations. Moreover, activation of these receptors in area postrema neurons boosts cAMP production, justifying use of $G\alpha_s$-coupled chemogenetic tools.

The areas postrema of *Glp1r-ires-Cre, Calcr-ires-Cre, Gfral-p2a-Cre*, and *Slc6a2-p2a-Cre* mice were injected with AAVs containing Cre-dependent genes encoding either a $G\alpha_s$-coupled DREADD-mCherry fusion protein (*AAV-Flex-*$G\alpha_s$*-DREADD*) or tdTomato (*AAV-Flex-tdTomato*) (Figure 3A). AAV injections preferentially labeled area postrema neurons, with modest labeling of nearby NTS neurons (Figure S3A) and exclusion of other potential expression sites including vagal ganglia (Figure S3B). cAMP imaging of area postrema neurons from *Glp1r-ires-Cre* mice injected with *AAV-Flex-*$G\alpha_s$*-DREADD* revealed CNO-

evoked cAMP transients in mCherry-positive neurons (67%, 8/12) but not mCherry-negative neurons (0%, 0/42) (Figure S3C). Furthermore, intraperitoneal CNO injection in mice expressing $G\alpha_s$-coupled DREADDs in area postrema GLP1R or CALCR neurons evoked Fos expression in mCherry-labeled neurons (Figure S3D).

Chemogenetic activation of various neuron subtypes was then elicited during a behavioral paradigm to measure conditioned flavor avoidance (Figure 3B). Water-restricted mice were given access to water containing saccharin and a fruit-flavored odor and then immediately injected with CNO. Half the conditioning trials involved cherry-flavored solution, and half involved grape-flavored solution, with mice displaying equal preference for both flavors in the absence of malaise induction (Figure S3E). Two days later, mice were tested in a two-choice preference assay comparing ingestion of cherry and grape solutions, and a preference index calculated as the time drinking the conditioned flavor divided by total time drinking. Control mice lacking DREADD expression (injected with *AAV-Flex-tdTomato*) across genotypes showed either no preference or a modest preference for the conditioned flavor (Figure 3C). In contrast, CNO-induced activation of DREADD-expressing GLP1R neurons, GFRAL neurons, or SLC6A2 neurons, but not CALCR neurons, during the training session caused later avoidance of the conditioned flavor in the test session (Figure 3C). We note that chemogenetic experiments involving $G\alpha_q$-coupled DREADDs in area postrema GLP1R neurons were similarly effective at conditioning flavor avoidance (Figure S3F) without increasing cAMP levels (Figure S3C), indicating that elevating multiple second messengers in AP neurons, including cAMP or calcium, can trigger behavioral responses. Together, these findings uncover functional specialization among area postrema neurons, as at least two excitatory neuron subtypes (clusters 2 and 4) provide a negative valence-teaching signal, while one subtype (cluster 1) does not.

In addition to causing behavioral avoidance, nausea is correlated with autonomic responses, so we measured physiological changes in response to optogenetic stimulation of area postrema neurons. *Glp1r-ires-Cre* mice were injected in the area postrema with an AAV encoding Channelrhodopsin (*AAV-Flex-ChR2*) or YFP (*AAV-Flex-Yfp*, control), and reporter expression confirmed (Figure S4A). Whole-cell voltage clamp recordings of dissociated ChR2-positive area postrema neurons revealed light-evoked currents (Figure S4B), and *in vivo* light stimulation evoked Fos expression in ChR2-positive area postrema neurons (Figure S4C).

Optogenetic activation of area postrema GLP1R neurons in anesthetized mice increased heart rate and blood pressure, had no effect on respiration, and evoked a complex change in gastric pressure that included increased tonic pressure and decreased phasic pressure (Figure S4D). Furthermore, optogenetic activation of a smaller neuronal group marked in *Slc6a2-p2a-Cre* mice produced similarly complex physiological responses (Figure S4E). The area postrema is known to influence autonomic physiology (Price et al., 2008), but whether such effects are secondary to nausea are debated (Borison, 1989). These data show that a small group of aversion-promoting area postrema neurons evokes a coordinated response that includes not only behavioral but also cardiovascular and gastrointestinal effects.

Area postrema GLP1R neurons condition flavor avoidance to peripheral poisons

Area postrema GLP1R neurons condition flavor avoidance, so we asked whether they were required for behavioral responses to viscerally introduced toxins. We used a genetic approach involving diphtheria toxin (DT) to ablate Cre-expressing area postrema neurons. Mouse cells are normally resistant to DT, but can be rendered susceptible by expression of the human DT receptor (DTR) from a Cre-dependent allele (*Rosa26-LSL-DTR*) (Buch et al., 2005). We expressed DTR in various area postrema neurons by crossing *Rosa26-LSL-DTR* mice to *Glp1r-ires-Cre, Gfral-p2a-Cre*, and *Slc6a2-p2a-Cre mice*, and then injected DT locally in the area postrema to eliminate Cre-expressing cells. Resulting mice were termed *Glp1r*-ABLATE^{AP}, *Gfral*-ABLATE^{AP}, and *Slc6a2*-ABLATE^{AP} mice respectively. We did not further investigate roles for area postrema CALCR neurons, since they did not condition aversion responses in chemogenetic experiments, and since multiple toxins evoked area postrema Fos responses in CALCR-negative neurons but not CALCR-positive neurons (Figure S5A). DT immunohistochemistry in *Glp1r*-ABLATE^{AP} mice revealed highly efficient and targeted cell ablation within the area postrema, as well as some cell loss in neighboring NTS regions, while other GLP1R neurons in the brain and vagal ganglia remained intact (Figure 4A).

Next, we tested various toxins for their ability to condition flavor aversion in *Glp1r*-ABLATE^{AP} mice (Figure 4B). Robust flavor avoidance was imposed by exendin-4, lithium chloride, lipopolysaccharide, or cisplatin in control Cre-negative *Rosa26-LSL-DTR* mice injected with DT (Non-ABLATE mice). However, *Glp1r*-ABLATE^{AP} mice failed to display flavor avoidance conditioned to exendin-4, lithium chloride, and lipopolysaccharide, while responses to cisplatin remained intact. We note that exendin-4 still decreased food intake in *Glp1r*-ABLATE^{AP} mice (Figure S5B), suggesting that at least partially distinct neural circuits mediate GLP1R-evoked appetite suppression and nausea. To determine whether toxin responses were mediated by particular GLP1R neuron subtypes, similar experiments were performed in *Slc6a2*-ABLATE^{AP} and *Gfral*-ABLATE^{AP} mice (Figure 4, S5C, S5D). Exendin-4 responses persisted following ablation of either SLC6A2 or GFRAL neurons, presumably because exendin-4 engages both cell types, either of which can condition aversion. In contrast, ablation of area postrema GFRAL neurons abolished lithium chloride- and lipopolysaccharide-conditioned aversion, so area postrema cell cluster 4 is required for behavioral responses to different malaise-inducing stimuli.

We next obtained mouse lines for Cre-dependent *Glp1r* knockout (*Glp1r*-KNOCKOUT^{Cre}) and Cre-dependent *Glp1r* rescue in the knockout background (*Glp1r*-RESCUE^{Cre}) (Sisley et al., 2014). We injected *AAV-Cre* into the area postrema of *Glp1r*-KNOCKOUT^{Cre} and *Glp1r*-RESCUE^{Cre} mice to generate *Glp1r*-KNOCKOUT^{AP} and *Glp1r*-RESCUE^{AP} mice respectively.

Control experiments involved *AAV-mCherry* injection to generate No-KNOCKOUT and No-RESCUE mice. RNA *in situ* hybridization for *Glp1r* mRNA revealed targeted elimination of *Glp1r* expression in *Glp1r*-KNOCKOUT^{AP} mice, and targeted restoration of *Glp1r* expression in *Glp1r*-RESCUE^{AP} mice (Figure 5A, S5E). Furthermore, peripheral exendin-4 induced area postrema Fos responses in No-KNOCKOUT and *Glp1r*-RESCUE^{AP} mice but not in No-RESCUE or *Glp1r*-KNOCKOUT^{AP} mice (Figure S5F).

Control No-KNOCKOUT mice avoided flavors paired with exendin-4 injection, while No-RESCUE mice did not. Area postrema-directed alterations in *Glp1r* expression reversed this behavior (Figure 5B) as *Glp1r*-RESCUE^{AP} mice displayed exendin-4-evoked flavor avoidance while *Glp1r*-KNOCKOUT^{AP} mice did not. Since low amounts of *AAV-Cre* could alter gene expression in vagal afferents that innervate the area postrema, we also generated *Glp1r*-RESCUE^{vagus} mice (*Glp1r*-RESCUE^{Cre} mice injected in vagal ganglia with *AAV-Cre*). Like No-RESCUE mice, *Glp1r*-RESCUE^{vagus} mice failed to display flavor avoidance conditioned to exendin-4 (Figure S5G, S5H). Taken together, these data indicate that exendin-4 induces malaise through GLP1R expressed in the caudal brainstem.

Subtype-specific projections of area postrema neurons

Only some area postrema neurons condition avoidance behavior, suggesting subtype-specific coupling to downstream neural circuits. We mapped neuronal projections of genetically defined area postrema neurons by injecting *AAV-Flex-tdTomato* into Cre knock-in mice, with a second marker allele, *Calca-gfp* (which marks CGRP neurons) or *Chat-gfp* (which marks cholinergic neurons) providing anatomical landmarks. First, we compared the projections of area postrema excitatory and inhibitory neurons using *Slc17a6-ires-Cre* (also known as *Vglut2-ires-Cre*) and *Gad2-ires-Cre* mice (Figure 6A). We observed excitatory projections to many brain regions, including the parabrachial nucleus (PBN), autonomic motor nuclei, and nearby NTS regions, similar to projections observed in prior bulk tracing studies (Borison, 1989; Miller and Leslie, 1994). Two-color analysis involving dual retrograde AAV injection in PBN and autonomic nuclei indicated that at least some excitatory neurons send collateral projections to multiple target nuclei (Figure S6A). In contrast, inhibitory projections were largely confined within the area postrema itself, and to a lesser extent within proximal NTS regions, but were not observed in the PBN or autonomic motor nuclei. Similar experiments in *Glp1r-ires-Cre, Calcr-ires-Cre, Gfral-p2a-Cre*, and *Slc6a2-p2a-Cre* mice revealed that each excitatory neuron subtype similarly projected to multiple output nuclei (Figure 6B, S6B, S6C).

Striking subtype-specificity was observed within the PBN. Interestingly, the PBN contains CGRP neurons which function as general alarm signals for many threats, including visceral malaise (Carter et al., 2015; Palmiter, 2018). GLP1R, GFRAL, and SLC6A2 neurons targeted a ventral PBN domain overlapping with cohorts of CGRP neurons (Figure 6C, S6D). In contrast, area postrema CALCR neurons displayed spatially distinct and bifurcated projections in the PBN, including a major dorsal branch remote from CGRP neurons, and a small ventral branch that overlapped with CGRP neurons only in anterior PBN (Figure 6C, S6D). Optogenetic stimulation of area postrema GLP1R neurons resulted in Fos expression in targeted PBN regions (Figure S7A), while ablation of area postrema GLP1R neurons diminished PBN Fos responses to lithium chloride and lipopolysaccharide (Figure S7B). Thus, PBN neurons receive inputs from area postrema GLP1R neurons, and require those inputs for toxin responses. Taken together, long-range projections from the area postrema are mostly excitatory, with neuronal subtypes that teach avoidance behavior (GFRAL and SLC6A2) sending dense projections near PBN CGRP neurons, providing a circuit-based explanation for observed aversion responses.

A neural circuit for aversion to therapeutic CASR agonists

A goal of these studies was to identify additional pathways to nausea, which could provide insight into the basic biology underlying nausea sensation, and potentially enable development of novel anti-nausea therapeutics. Single-cell transcriptome data revealed many other cell surface receptor genes to be expressed in area postrema excitatory neurons (Figure 1D). Introduction of a foreign GPCR into area postrema GLP1R neurons rendered ligands for that receptor capable of conditioning flavor avoidance (Figure 3C). We reasoned that ligands for endogenous area postrema receptors might exert similar behavioral effects. For example, transcriptome data revealed that the calcium sensing receptor gene (*Casr*) was highly expressed in excitatory neuron clusters 2 and 4 (Figure 7A), two neuron types that condition aversion. Interestingly, the CaSR agonist cinacalcet is used clinically, with patients anecdotally reporting nausea as a side effect (Lindberg et al., 2005). However, the neural basis for cinacalcet-induced nausea has been unexplored, with potential roles for any of several periphery-to-brain pathways.

RNA *in situ* hybridization revealed abundant *Casr* mRNA in subsets of area postrema neurons (Figure 7B). Two-color expression analysis indicated that *Casr* mRNA was expressed in area postrema neurons marked in *Glp1r-ires-Cre; Rosa26-LSL-L10GFP* mice, but not in *Calcr-ires-Cre; Rosa26-LSL-L10GFP* mice (Figure 7C), consistent with transcriptomic data. CaSR agonists increase intracellular calcium levels in some cells (Tfelt-Hansen and Brown, 2005), and we observed that elevating intracellular calcium levels in area postrema GLP1R neurons with a $G\alpha_q$-coupled DREADD evoked flavor avoidance (Figure S3F). Intraperitoneal cinacalcet injection induced Fos expression in area postrema neurons, with responses largely restricted to GLP1R neurons (Figure 7D). Using the conditioned flavor avoidance paradigm, we observed that cinacalcet administration indeed provided an aversive teaching signal in wild-type mice (Figure 7E), and moreover, that ablation of area postrema GLP1R neurons in *Glp1r*-ABLATE^{AP} mice eliminated this behavioral response (Figure 7F). Thus, cinacalcet-evoked aversion involves CaSR agonism in the same area postrema neurons engaged by GLP1R agonists. Together, these findings suggest a general model that nausea-associated behaviors are evoked by agonists of any cell surface receptor that 1) is expressed in defined area postrema neurons, and 2) can engage particular intracellular second messengers, which can include cAMP or calcium.

DISCUSSION

The brain receives sensory inputs through multiple pathways. External sensory neurons mediate our basic senses of smell, touch, taste, vision, and hearing, while various internal sensory neurons relay inputs from organs and tissues within the body. In addition, sensory circumventricular organs, such as the area postrema, reside within the brain proper and can function in interoception by detecting humoral cues at privileged anatomical locations outside the blood-brain barrier.

Here, we used single-nucleus RNA sequencing to create an atlas of area postrema neurons. We identified four excitatory and three inhibitory neuron types, and assembled genetic tools to map, image, and control several of them. Chemogenetics revealed two subpopulations of excitatory GLP1R neurons that provide aversive teaching signals, one marked by GFRAL

(cluster 4) and another by the noradrenaline transporter SLC6A2 (cluster 2). Ablating area postrema GLP1R neurons eliminated flavor avoidance conditioned to multiple stimuli, including exendin-4, lithium chloride, and lipopolysaccharide. GLP1R neurons engage multiple downstream brain regions, consistent with a prior model that motor control of nausea/vomiting is not thought to involve a regionalized center, but rather a distributed neural network, with each nucleus mediating a particular aspect of the coordinated motor program (Hornby, 2001). Some division of labor among area postrema neurons is revealed, with GFRAL neurons but not SLC6A2 neurons necessary for lithium chloride responses. Furthermore, not all area postrema neurons evoke identical behavioral responses, as cluster 1 neurons (marked in *Calcr-ires-Cre* mice) do not provide an aversion teaching signal, and also display spatially distinct projections to the PBN, suggesting engagement of distinct downstream neural circuits.

Single-cell RNA sequencing also revealed a diversity of cell surface receptors expressed in area postrema neurons. For example, cluster 4 neurons express genes encoding GLP1R, GFRAL, and CaSR, as well as other receptors, suggesting that multiple signals of visceral malaise can be funneled through these neurons to evoke complex nausea-associated responses. We observed a) robust Casr expression in cell clusters 2 and 4, b) that the CaSR agonist cinacalcet activated area postrema GLP1R neurons and induced flavor avoidance in mice, and c) that ablation of area postrema GLP1R neurons eliminated cinacalcet-evoked aversion. Several disease conditions elevate plasma calcium, termed hypercalcemia, and cause nausea and vomiting; our work suggests that such adverse responses are likely mediated by area postrema CaSR. Moreover, cluster 2 and 4 neurons express genes for several orphan receptors, and it seems possible that agonists for these receptors, once discovered, would also cause nausea.

Cell surface receptors in cluster 4 area postrema neurons can engage divergent intracellular signaling pathways. For example, GLP1R and CaSR are GPCRs that increase intracellular cAMP and calcium levels respectively, while GFRAL signals through the tyrosine kinase receptor Ret, (Emmerson et al., 2017; Hsu et al., 2017; Mullican et al., 2017; Yang et al., 2017). Furthermore, activation of either $G\alpha_s$-coupled or $G\alpha_q$-coupled DREADDs in area postrema GLP1R neurons is sufficient to condition flavor avoidance. cAMP and calcium can exert many downstream effects that could lead to neuronal depolarization, and cAMP is used as a second messenger in external sensory neurons; for example, cyclic nucleotide-gated channels mediate odor transduction in olfactory sensory neurons (Brunet et al., 1996). Perhaps any receptor can provide a danger signal as long as it 1) is expressed in the correct area postrema neurons, and 2) couples to appropriate intracellular signaling pathways, such as cAMP or calcium in cluster 4 neurons. The ability of area postrema neurons to channel diverse types of stimuli into an aversive response would seemingly provide evolutionary flexibility in acquiring new signals of malaise.

The interplay between vagal afferents and area postrema neurons in nausea remains an open question. A vagal route for detection of peripheral malaise would presumably be faster and not require toxin/pathogen absorption into circulation, while a humoral route might be engaged only when danger signals have entered the bloodstream, indicating that a threat can no longer be locally contained. For some emetic stimuli, the area postrema may simply relay

vagal inputs; however, other humoral cues, such as GDF15, act directly through specific receptors located in the area postrema (Emmerson et al., 2017; Hsu et al., 2017; Mullican et al., 2017; Yang et al., 2017). Our work here involving region-specific gene knockout and rescue indicates that GLP1R acts in the area postrema rather than the vagus nerve or other locations to mediate nausea-associated behaviors. For comparison, vagal GLP1R neurons function as mechanoreceptors in the stomach and intestine (Williams et al., 2016), and knockout of vagal GLP1R does not impact anorectic effects of GLP1R agonists (Sisley et al., 2014). Furthermore, these findings suggest at least a partial separation of neural pathways that mediate satiety and nausea to exendin-4, consistent with a model that feeding inhibition involves GLP1R neurons in several brain regions (Adams et al., 2018; Burmeister et al., 2017; Fortin et al., 2020; Ghosal et al., 2017; Secher et al., 2014) while aversion involves a more focal brainstem response. Selective control of particular GLP1-responsive neural circuits could in principle dissociate the therapeutic effects of GLP1R agonism from harmful side effects.

Area postrema cell type four expresses *Gfral*, conditions avoidance upon chemogenetic activation, and mediates aversion to visceral lithium chloride and lipopolysaccharide. Area postrema neurons presumably do not detect toxins directly, but instead are activated by secondary damage-associated signals that arrive through humoral and/or vagal routes. The GFRAL agonist GDF15 is a circulating hormone that has garnered significant clinical interest for its ability to induce weight loss (Tsai et al., 2018). It has been debated whether GDF15-induced weight loss is due to induction of nausea; GDF15-evoked aversion and emesis have been observed in some studies but not others (Borner et al., 2020; Day et al., 2019; Mullican et al., 2017; Patel et al., 2019). Intriguingly, GDF15 expression is induced by the cellular integrated stress response (Patel et al., 2019), and many sickness-associated stimuli lead to increased serum levels of GDF15, including cancer cachexia, bacterial and viral infection, cisplatin, lithium chloride, bacterial lipopolysaccharide, and pregnancy (Luan et al., 2019; Tsai et al., 2018), raising the possibility that GDF15-responsive neurons provide a general alarm signal engaged by multiple manifestations of visceral malaise. Studies here involving activation of area postrema GFRAL neurons suggest that using GFRAL agonists to lower body weight in human patients would carry risk of evoking nausea. We note that cisplatin also induces GDF15 production (Hsu et al., 2017), but cisplatin-induced flavor avoidance persisted after ablation of area postrema GLP1R neurons (which includes GFRAL neurons), suggesting a parallel neuronal response pathway (Horn, 2009).

Single-nucleus RNA sequencing additionally revealed other area postrema neuron types of unknown function. Cluster 2 neurons marked in *Slc6a2-p2a-Cre* mice also project to CGRP neurons in the PBN and provide an aversive teaching signal. Furthermore, different inhibitory neurons express receptors for the gut hormones ghrelin and GIP, and project locally within the area postrema. Future studies will reveal the connections of area postrema inhibitory neurons, and whether they exert state-dependent control over, and possibly suppression of, excitatory area postrema neurons involved in nausea or other behaviors.

The identification of neurons that mediate hunger, thirst, and other internal states were pivotal advances in neuroscience, providing genetic access to neural circuits that control aspects of animal behavior. The sensation of nausea has remained essentially uncharted in

comparison. Here, we report the identification of area postrema neurons that evoke nausea-related behaviors in mice, and show that aversive behaviors can be suppressed through cell-specific manipulations. Revealing area postrema cell types and receptors that sense signals of visceral malaise may help in the identification of new therapies for nausea, a major clinical need.

STAR METHODS

RESOURCE AVAILABILITY

Lead contact—Further information and requests for resources and reagents should be directed and will be fulfilled by the Lead Contact, Stephen Liberles (Stephen_Liberles@hms.harvard.edu).

Materials Availability—Reagents and mouse lines generated in this study, including *Gfral-p2a-Cre* and *Slc6a2-p2a-Cre* mice, will be available from the lead contact. *Glp1r*-RESCUE^{Cre} mice were an unpublished gift from Randy Seeley (University of Michigan) and material requests should be directed to seeleyrj@med.umich.edu.

Data and code availability—Single-cell transcriptome data from area postrema neurons are available through GEO (accession number GSE160938); codes for bioinformatics analysis are available in GitHub (http://github.com/jakaye/AP_scRNA); other primary images and data are available at Mendeley (doi:10.17632/tpw4c3g9m3.1).

EXPERIMENTAL MODEL AND SUBJECT DETAILS

All animal husbandry and procedures followed the ethical guidelines outlined in the NIH Guide for the Care and Use of Laboratory Animals (https://grants.nih.gov/grants/olaw/guide-for-the-care-and-use-of-laboratory-animals.pdf), and all protocols were approved by the institutional animal care and use committee (IACUC) at Harvard Medical School. *Slc6a2-p2a-Cre* and *Gfral-p2a-Cre* mice were constructed as described below; *Glp1r-ires-Cre* (Williams et al., 2016), *Calcr-ires-Cre* (Pan et al., 2018), and *Slc17a6-ires-Cre* (Vong et al., 2011) mice were described before; mouse lines for cell-specific deletion and rescue of *Glp1r* were gifts from Randy Seeley (University of Michigan) (Sisley et al., 2014); *Calca-gfp* mice were from GENSAT; wild-type C57BL/6J (000664), *Rosa26-LSL-L10GFP* (024750), *Chat-gfp* (007902), *Rosa26-LSL-tdTomato* (007908), *Gad2-ires-Cre* (010802), and *Rosa26-LSL-DTR* (007900) mice were purchased (Jackson Laboratory). Single-cell sequencing was performed on male C57BL/6J mice; both male and female mice between 8-24 weeks old were used for all other studies, and no differences based on sex were observed.

METHOD DETAILS

Single-nucleus RNA sequencing—Brains were acutely harvested from 30 adult male C57BL/6J mice (two technical replicates). Coronal brain slices (250 mm, Leica VT1000S vibratome) containing the area postrema (AP) were placed in artificial cerebral spinal fluid (ACSF, 4°C) solution [ACSF solution: (in mM) 126 NaCl, 3 KCl, 20 $NaHCO_3$, 1.25 NaH_2PO_4, 2 $MgCl_2$, 20 D-glucose, 2 $CaCl_2$, 0.0001 tetrodotoxin, 0.02 6,7-

dinitroquinoxaline-2,3-dione, 0.05 DL-2-amino-5-phosphonovaleric acid continually bubbled with carbogen gas (95%O_2 / 5%CO_2)]. The area postrema was visualized by microscopy and harvested based on anatomical landmarks. Harvested tissue was homogenized (4°C) in buffer containing 0.3% IGEPAL CA-630 and protease inhibitor cocktail (Biotool B14011), and (in mM) 250 sucrose, 25 KCl, 20 $NaHCO_3$, 1.25 NaH_2PO_4, 5 $MgCl_2$, 20 Tricine-KOH, 0.15 spermine, 0.5 spermidine, and 1 dithiothreitol. Samples were filtered (40 μM strainers), diluted with iodixanol (25% final concentration) and layered on an iodixanol gradient (30% and 40% iodixanol containing 0.04% BSA and RNasin (Promega N2611,64 units/ml). Samples were centrifuged (18 min, 10,000 g, 4°C) and nuclei collected at the 30-40% iodixanol interface. Nuclei were individually encapsulated (~3,000 in each of 2 replicates) in small droplets using an inDrop platform with v3 chemistry hydrogels, and cDNA was prepared from individual nuclei (Zilionis et al., 2017). cDNA was sequenced (Illumina NextSeq 500, High Output v2). For transcriptome analysis, nuclei barcodes and unique transcript reads (UMIs) were assigned using zUMIs v2.8.0 pipeline with intronic reads enabled (Parekh et al., 2018). Reads were aligned to a modified Ensembl mm10 mouse reference genome with STAR v2.7.3. For analysis, 3' UTRs were extended for *Glp1r, Ghsr, Prhlr*, and *Prokr2* genes with area postrema expression where associated reads occurred outside the annotated region. Raw count matrices were analyzed in R v3.6.0 using Seurat v3.1.5 (Butler et al., 2018; Satija et al., 2015). The UMI count matrix was filtered based on barcode quality, the number of unique transcripts, the number of total genes, and the number of total reads for every gene detected. The filtered UMI count matrix was transformed and batch effects were regressed out using SCTransform (Hafemeister and Satija, 2019). Transformed matrices were then used for principal component analysis, differential gene expression analysis, cell type clustering, and generating UMAP plots. Clusters containing both neural and glial markers were removed from analysis, which were presumed to be multiple nuclei encapsulated in one droplet. Once identified among all nuclei, neuronal nuclei were re-analyzed separately. Subsets of nuclei were reprocessed with SCTransform from raw counts. Signature genes were based on adjusted p-value scores (Wilcoxon-Ranked Sum test) indicating differential expression, and identified from genes expressed in <12.5% of other cells. Additional parameters used in the bioinformatic pipeline are available on GitHub (http://github.com/jakaye/AP_scRNA).

Mouse genetics—*Gfral-p2a-Cre* and *Slc6a2-p2a-Cre* mice were generated by pronuclear injection of Cas9 protein, CRISPR sgRNAs targeting the *Gfral* or *Slc6a2* locus 3’ UTR, and a single strand DNA template containing a *p2a-cre* cassette with 150 bp homology arms into C57BL/6 embryos.

Transgenic pups were screened by PCR analysis, and correct expression of the transgene was verified by RNA *in situ* hybridization or immunostaining. All Cre driver lines used are viable and fertile, and abnormal phenotypes were not detected. Genotyping primers for *Gfral-p2a-Cre* mice were TCTGGGAACTTTATGCTCAGGAA (common 5’ primer), TCACACAGACATGTGGTTGGT (WT allele 3’ primer), and AGGTTCTGCGGGAAACCATT (*p2a-Cre* allele 3’ primer), with differentially sized PCR products for the wild-type allele (460 bp) and knock-in allele (228 bp) in two separate reactions. Genotyping primers for *Slc6a2-p2a-Cre* mice were:

GGGGTGGTTTCTTTGCATCC (common 5' primer), ATGGGTTCCTCCTCCTCCTC (WT allele 3' primer), and CGCGCGCCTGAAGATATAGA (*p2a-Cre* allele 30 primer), with differentially sized PCR products for the wild-type allele (239 bp) and knock-in allele (513 bp) in two separate reactions.

cAMP imaging of area postrema neurons—Neuronal responses were measured in acutely dissociated area postrema neurons. Area postrema tissue was harvested, digested with a papain dissociation system (Worthington Biochemical, LK003150, 60 min, 37°C), washed [Earle's Balanced Salt Solution containing ovomucoid protease inhibitor (1 mg/ml), BSA (1 mg/ml), and DNase (100 units/ml)], and gently triturated with three pipettes of decreasing diameters. Isolated single cells were centrifuged (100g, 5 min, 4°C) and resuspended in culture medium [Neurobasal medium with 2.5% fetal bovine serum, N-2 (Thermo Fisher 17502048), B-27 (Thermo Fisher 17504044), Glutamax (Thermo Fisher 35050061), and Antibiotic-Antimycotic (Thermo Fisher 15240062)]. Cells were plated on laminin-coated coverslips (neuVitro, GG-12-Laminin), and transfected (overnight, 37°C) with a viral vector encoding Green Up cADDis cAMP sensor (Montana Molecular U0200G). Real-time cAMP transients were imaged using a Leica SP5 II confocal microscope with cells under continuous gravity-based perfusion (0.6 ml/min flow rate, 1 ml chamber reservoir) of Ringer's solution (in mM 140 NaCl, 5 KCl, 2 MgCl2, 2 CaCl2, 10 HEPES, 10 glucose, pH 7.4) alone or containing test stimuli. The baseline activity for each neuron was defined as the average fluorescence green intensity over a five-minute period preceding stimulus delivery, and cells were excluded if they failed to display responses to positive controls. Image stacks were analyzed with FIJI (Schindelin et al., 2012).

AAV/DT injections—Mice were anaesthetized (avertin) and placed on a stereotaxic frame (David Kopf Instruments) with heads facing down ~45°. The fourth ventricle and area postrema were surgically exposed after removal of the meninges, and a Nanoject III Injector (Drummond) was positioned directly into the area postrema for injections of virus (titer ≥ 10^{13} vg/ml, 35 nl, 2 nl/second) or DT (Sigma D0564, 5 μg/ml in saline, 35 nl, 2 nl/second). Dual injection of retrograde virus (titer ≥ 10^{13} vg/ml) was done in the PBN (anterior-posterior: −5.23 mm; medial-lateral: 1.45 mm; dorsal-ventral: 2.45 mm from brain surface, 200 nl, 1 nl/sec) and VLM (anterior-posterior: −7.52 mm; medial-lateral: 1.3 mm; dorsal-ventral: 4.5 mm from brain surface, 100 nl, 1 nl/sec). Animals recovered for 3-4 weeks for behavioral or expression analysis, or 2 weeks for subsequent surgery to implant optic fibers. Injected viruses included *AAV-Flex-tdTomato* (Addgene, *AAV9-CAG-Flex-tdTomato*, prep #51503-AAV9) (Oh et al., 2014), *AAV-Flex-ChR2* (Addgene, *AAV9-Ef1a-DIO-hChR2(H134R)-mCherry*, prep #20297-AAV9), *AAV-Flex-Gα$_s$-DREADD* (Addgene, *AAV-hSyn-DIO-rM3D (Gα$_s$)-mCherry*, plasmid 50458, custom virus, serotype 9), *AAV-Flex-Gα$_q$-DREADD* (Addgene, *AAV-hSyn-DIO-hM3D(Gα$_q$)-mCherry*, plasmid #44361, custom virus prepared at Boston Children's Hospital Viral Core, serotype 8) (Krashes et al., 2011), *AAV-Flex-Yfp* (Addgene, *AAV9-Ef1a-DIO-EYFP*, prep #27056-AAV9), *AAV-Cre* (SignaGen, *AAV1-CAG-Cre-mCherry), AAV-mCherry* (SignaGen, *AAV1-CAG-mCherry*), *AAVretro-Flex-tdTomato* (Addgene, *AAVrg-Flex-tdTomato*, prep #28306-AAVrg), and *AAVretro-Flex-GFP* (Addgene, *AAVrg-hSyn-DIO-GFP*, prep #50457-AAVrg). The plasmid for *AAV-Flex-Gα$_s$-DREADD* was transfected into HEK-293 cells together with Rep/Cap

(serotype 9) and helper plasmids (Addgene) using polyethylenimine (Polysciences, 239661). Three days later, virus was collected and purified by iodixanol gradient ultracentrifugation (according to the Addgene AAV preparation protocol). After behavioral measurements, tissue was collected to determine ablation efficiency by DTR immunohistochemistry or viral reporter expression.

Analysis of RNA, protein, and reporter expression—RNA *in situ* hybridization (ISH) was performed on coronal brain (25 μm) or vagal ganglia (12 μm) cryosections of unfixed tissue as described previously (Prescott et al., 2020) with minor modifications. Colorimetric ISH involved digoxigenin-conjugated cRNA riboprobes, alkaline phosphatase-conjugated anti-digoxigenin antibody (Roche 11093274910) and staining with NBT/BCIP (Thermo Scientific 34042). Fluorescent *in situ* hybridization involved digoxigenin-conjugated cRNA riboprobes, peroxidase-conjugated anti-digoxigenin antibody (Roche 11207733910) and TSA-Cy5.5 (Perkin-Elmer NEL766001KT). High-stringency washes used 5X SSC (2x5 minutes, 70°C, VWR 45001-046) and 0.2X SSC (2x30 minutes, 70°C) and subsequent washes and antibody incubations used PBS buffer with 0.05% Tween-20. Phosphatase and peroxidase reporter reactions were performed according to manufacturer's protocols. Fluorescent images were analyzed with a Leica SP5 II confocal microscope, and colorimetric images were analyzed with a Nikon Ti2 Inverted microscope. cRNA probes were synthesized with digoxigenin-conjugated (Roche 11277073910) dNTPs and transcribed *in vitro* following manufacturer's protocols (MegaScript T7 or T3 Kits, Invitrogen AM1334 or AM1338). Probes (listed 5' to 3') were amplified using the following primer pairs: *Glp1r* (1392 bp) ATGGCCAGCACCCCAAGC and TCAGCTGTAGGAACTCTGG, *Calcr* (1009bp) AAGATCCAGTGGAGCCAACG and GCTAGATAGCACCCAAGGGC, *Slc6a2* (1016bp) GGGCGTTAGGCAGAAACTCT and CCTCCATGGGACATGGGAAC, *Casr* (812bp) CAGCATGCTCATCTTCTTCATC and AGGAGTGCAGTATGTTTTCCGT.

Immunohistochemistry and reporter fluorescence analysis was performed on cryosections (40 μm) of tissues fixed by intracardial perfusion with cold fixative (4% paraformaldehyde, PBS) and cryopreserved (30% sucrose, PBS, 4°C, two days) or on wholemounts of vagal ganglia (Figure 4A, S3B). Slide-mounted sections were blocked (1 hr, RT, blocking solution: PBS, 5% donkey serum, 0.1% Triton X-100), incubated with primary antibody (blocking solution, 4°C, overnight), washed (PBST, 3x5 min, RT), incubated with fluorophore-conjugated secondary antibodies (1:500, PBST, 5% donkey serum, 1-2 hours, RT). Antibody solutions were Rabbit-anti-RFP (for tdTomato, Rockland AB_2209751, 1:1000), Goat-anti-HB-EGF (for DTR, R&D Systems AF-259-NA, 1:500), Rabbit-anti-Fos (Synaptic Systems 226003, 1:1000), and Anti-GFR alpha-like antibody (for GFRAL, R&D Systems AF5728, 1:500). Fos inductions involved injection (IP, 10 μl/g) of either CNO (0.1 mg/ml), LiCl (0.4 M), LPS (5 μg/ml), cinacalcet (1.5 mM), or saline alone. After 2.5 hours the animals were sacrificed by intracardial perfusion of fixative for immunohistochemical analysis. Fluorogold (fluorescence was measured in fixed cryosections three days after injection (IP, Santa Cruz sc-358883, 1% in saline, 5 μl/g). For Figure 4A, whole mount immunostaining was performed on fixed nodose ganglia that were first permeabilized (11.5 g glycine, 400 mL PBS with 0.2% Triton-X, 100 mL DMSO, 37°C, one week). Fluorescent images were

analyzed with a Leica SP5 II confocal microscope, and colorimetric images were analyzed with a Nikon Ti2 Inverted microscope.

Behavioral assays—Conditioned flavor avoidance assays involved a six-day protocol with daily 30-minute introductions to a test arena containing two water bottles soon after dark onset. Mice were water restricted in the home arena, but given *ad libitum* water access in the test arena. In the first three days (habituation days), both water bottles contained unflavored water. On day four (conditioning day), both water bottles were filled with either grape-flavored or cherry-flavored water (grape or cherry Kool-Aid) sweetened with 0.2% saccharin, each on half of trials. Immediately after test arena occupancy on the conditioning day, mice were injected with saline (10 μl/g, IP) alone or containing either CNO (0.1 mg/ml), exendin-4 (1.43 μM), LiCl (0.4 M), LPS (5 μg/ml), cisplatin (0.75 mg/ml), or cinacalcet (1.5 mM). On day five (recover day), both water bottles contained unflavored water. On day six (testing day), one water bottle contained cherry-flavored water, while the other contained grape-flavored water on a randomized arena side, and consumption from each water bottle scored using an automated lickometer, design based on (Slotnick, 2009).

Food intake was measured in home cages with ad libitum access to water and food. Animals were habituated for seven days to feeding from a ceramic bowl (replaced daily with 8 grams of food prior to dark onset). Five minutes before dark onset on the test day, animals were injected with saline (10 μl/g, IP) alone or containing exendin-4 (1.43 μM). A fresh ceramic bowl with food (8 g) was given, and the amount of uneaten food remaining was weighed at various time points.

Physiological measurements—Mice previously injected with *AAV-Flex-ChR2* or *AAV-Flex-eYfp* were anesthetized (urethane, 2 mg/g) and body temperature (37°C) was maintained with a heating pad. For optogenetic stimulation, the area postrema was surgically exposed and positioned beneath an optic fiber (200 mm core, Thorlabs) coupled to a DPSS laser light source (473 nm, 150 mW, Ultralaser). Illumination was controlled by a shutter system (Uniblitz) with equivalent results observed to two settings (6 mW, 2 min, 5 Hz, 50 ms pulses or 6 mW, 2 min, 20 Hz, 5 ms pulses). Heart rate was determined by electrocardiogram amplifier (Biopac, ECG100C); breathing rhythms by tracheal pressure measurements taken on a differential pressure transducer (Harvard Apparatus, Part.No 73-0064); gastric pressure through a pressure transducer (Biopac TSD104A) inserted in the stomach after the stomach was flushed of contents and filled with PBS to maintain constant baseline pressure; blood pressure through a pressure transducer cannulated to the carotid artery (Biopac TSD104A). All signals were acquired using a data acquisition system (Biopac MP150); respiratory rhythms and heart rate were transformed to beats per minute, using the Acqknowledge program (ver. 5.0.1). Tonic and phasic components of gastric pressure were computationally isolated using a Kaiser window to separate high and low frequency signals. Light-evoked responses were measured by whole-cell patch-clamp recordings of harvested area postrema neurons two hours after attachment using a Molecular Device 700B amplifier with filtering at 1 kHz and 4–10 mΩ electrodes filled with an internal solution containing (in mM) 130 K-Gluconate, 15 KCl, 4 NaCl, 0.5 $CaCl_2$, 10 HEPES, 1 EGTA, pH 7.2, 290 mOsm. External solution contained (in mM) 150 NaCl, 2.8 KCl, 1

$MgSO_4$, 1 $CaCl_2$, 10 HEPES, pH 7.4, 300 mOsm. For Fos induction studies, mice previously injected with *AAV-Flex-ChR2* underwent surgery to implant optic fibers (Mono Fiberoptic Cannula, Doric Lenses) above the area postrema (anterior-posterior: −7.56 mm; medial-lateral: 0 mm; dorsal-ventral 3.5 mm from the brain surface); the fiber optic cannula was affixed to the skull with C&B Metabond (Parkell) and dental acrylic, and animals recovered for an additional week. Mice were placed in cages with no cage tops, and fiber optic cables (1 m long, 500 μm diameter; Goldstone Scientific) coated with opaque heat-shrink tubing were firmly attached to the implanted cannula with zirconia sleeves (Doric Lenses). Photostimulation involved light pulses (5 Hz LED, 1 hour) and the animal was immediately sacrificed for immunohistochemical analysis.

QUANTIFICATION AND STATISTICAL ANALYSIS

Graphs represented data as mean ± SEM, as indicated in figure legends. All data points are derived from different mice except for some data points related to expression quantification (Figure 4A, S3A, S4A, S5D, S5E, S5H, S7B) which include multiple sections per mouse.

Sample sizes from left to right: Figure 3C (10, 15, 6, 6, 9, 9, 10, 5), Figure 4A (7, 10, 8, 12, 8, 21, 7, 15, 4, 18, 6, 10), Figure 4B (12, 8, 7, 7, 17, 4, 7, 13, 18, 8, 9, 6, 12, 6, 4), Figure 5B (11, 12, 18, 16), Figure 7E (11, 14), Figure 7F (16, 10), Figure S3A (9, 6, 9, 6, 3, 6, 3, 6, 6, 20, 6, 11, 9, 6, 9, 6), Figure S3E (14), Figure S3F (8, 5), Figure S4A (7, 6, 7, 6, 9, 20, 9, 11), Figure S4E (5, 4; 5, 4, 5; 5, 7, 4; 6, 14, 4; 4, 6, 3), Figure S5B (6, 6, 8, 3; 6, 6, 8, 3; 6, 6, 8, 3; 6, 6, 8, 3), Figure S5D (3, 10, 8, 11, 8, 12, 12, 13), Figure S5E (7, 7, 6, 6, 7, 7, 10, 10), Figure S5F (7, 7), Figure S5H (4, 9, 7), Figure S7B (14, 26, 19, 19, 8, 6).

In neuronal imaging experiments, cells were counted as responsive if stimulus-evoked $\Delta F/F$ exceeded three standard deviations above the baseline mean. Physiological changes were calculated by comparing responses during light stimulation (two minutes) to the two-minute period preceding stimulation. Statistical significance was measured on MATLAB (MathWorks) using a two-way mixed ANOVA with Tukey's multiple comparison post hoc analysis (Figure 3C), or on Prism 7 software (Graphpad) using a Kruskal-Wallis test with Dunn's multiple comparison (Figure 5), a Kruskal-Wallis test with Dunn's multiple comparison and Holm-Sidak correction (Figure 4B), a Mann-Whitney test with Bonferroni correction (Figure 4A, S5D, S5E, S5H, S7B), a Mann-Whitney test (Figure 7, S3, S4E left, S5G), a one-way ANOVA with post hoc Dunnett's multiple comparison tests (Figure S4 except S4E left), or a two-way repeated-measures ANOVA with Tukey's multiple comparison post hoc analysis (Figure S5B).

Supplementary Material

Refer to Web version on PubMed Central for supplementary material.

ACKNOWLEDGMENTS

We thank David Julius, Brad Lowell, Charles Horn, Marie Bao, and Liberles lab members for manuscript comments, David Ginty, Brad Lowell, Randy Seeley, Martin Myers, and David Olson for mice, Benjamin Umans and Rachael Brust for automated behavioral analysis, the HMS Nikon Imaging Center for microscopy assistance, the ICCB Single Cell Core for assistance with InDrop experiments, the HMS Biopolymers Facility for sequencing, and the HMS O2 High Performance Computer Cluster for bioinformatics support. The work was funded by NIH

grants to SDL (DP1 AT009497 and R01 DK103703) and a training grant supporting JAK (T32 HL007901). CZ is a fellow of the Damon Runyon Cancer Research Foundation. SLP is an Open Philanthropy Fellow of the Life Sciences Research Foundation. SDL is an investigator of the Howard Hughes Medical Institute.

REFERENCES

Adams JM, Pei H, Sandoval DA, Seeley RJ, Chang RB, Liberles SD, and Olson DP (2018). Liraglutide Modulates Appetite and Body Weight Through Glucagon-Like Peptide 1 Receptor-Expressing Glutamatergic Neurons. Diabetes 67, 1538–1548. [PubMed: 29776968]

Andrews PL (1992). Physiology of nausea and vomiting. Br J Anaesth 69, 2S–19S. [PubMed: 1486009]

Baggio LL, and Drucker DJ (2007). Biology of incretins: GLP-1 and GIP. Gastroenterology 132, 2131–2157. [PubMed: 17498508]

Barth SW, Riediger T, Lutz TA, and Rechkemmer G (2004). Peripheral amylin activates circumventricular organs expressing calcitonin receptor a/b subtypes and receptor-activity modifying proteins in the rat. Brain research 997, 97–102. [PubMed: 14715154]

Borison HL (1989). Area postrema: chemoreceptor circumventricular organ of the medulla oblongata. Progress in neurobiology 32, 351–390. [PubMed: 2660187]

Borner T, Shaulson ED, Ghidewon MY, Barnett AB, Horn CC, Doyle RP, Grill HJ, Hayes MR, and De Jonghe BC (2020). GDF15 Induces Anorexia through Nausea and Emesis. Cell Metab 31, 351–362 e355. [PubMed: 31928886]

Brunet LJ, Gold GH, and Ngai J (1996). General anosmia caused by a targeted disruption of the mouse olfactory cyclic nucleotide-gated cation channel. Neuron 17, 681–693. [PubMed: 8893025]

Buch T, Heppner FL, Tertilt C, Heinen TJ, Kremer M, Wunderlich FT, Jung S, and Waisman A (2005). A Cre-inducible diphtheria toxin receptor mediates cell lineage ablation after toxin administration. Nature methods 2, 419–426. [PubMed: 15908920]

Burmeister MA, Ayala JE, Smouse H, Landivar-Rocha A, Brown JD, Drucker DJ, Stoffers DA, Sandoval DA, Seeley RJ, and Ayala JE (2017). The Hypothalamic Glucagon-Like Peptide 1 Receptor Is Sufficient but Not Necessary for the Regulation of Energy Balance and Glucose Homeostasis in Mice. Diabetes 66, 372–384. [PubMed: 27908915]

Butler A, Hoffman P, Smibert P, Papalexi E, and Satija R (2018). Integrating single-cell transcriptomic data across different conditions, technologies, and species. Nature biotechnology 36, 411–420.

Carpenter DO, Briggs DB, Knox AP, and Strominger N (1988). Excitation of area postrema neurons by transmitters, peptides, and cyclic nucleotides. J Neurophysiol 59, 358–369. [PubMed: 2895167]

Carter ME, Han S, and Palmiter RD (2015). Parabrachial calcitonin gene-related peptide neurons mediate conditioned taste aversion. J Neurosci 35, 4582–4586. [PubMed: 25788675]

Day EA, Ford RJ, Smith BK, Mohammadi-Shemirani P, Morrow MR, Gutgesell RM, Lu R, Raphenya AR, Kabiri M, McArthur AG, et al. (2019). Metformin-induced increases in GDF15 are important for suppressing appetite and promoting weight loss. Nature Metabolism 1, 1202–1208.

Emmerson PJ, Wang F, Du Y, Liu Q, Pickard RT, Gonciarz MD, Coskun T, Hamang MJ, Sindelar DK, Ballman KK, et al. (2017). The metabolic effects of GDF15 are mediated by the orphan receptor GFRAL. Nat Med 23, 1215–1219. [PubMed: 28846098]

Ferguson AV, and Bains JS (1996). Electrophysiology of the circumventricular organs. Front Neuroendocrinol 17, 440–475. [PubMed: 8905349]

Fortin SM, Lipsky RK, Lhamo R, Chen J, Kim E, Borner T, Schmidt HD, and Hayes MR (2020). GABA neurons in the nucleus tractus solitarius express GLP-1 receptors and mediate anorectic effects of liraglutide in rats. Sci Transl Med 12.

Ghosal S, Packard AEB, Mahbod P, McKlveen JM, Seeley RJ, Myers B, Ulrich-Lai Y, Smith EP, D'Alessio DA, and Herman JP (2017). Disruption of Glucagon-Like Peptide 1 Signaling in Sim1 Neurons Reduces Physiological and Behavioral Reactivity to Acute and Chronic Stress. J Neurosci 37, 184–193. [PubMed: 28053040]

Habib N, Li Y, Heidenreich M, Swiech L, Avraham-Davidi I, Trombetta JJ, Hession C, Zhang F, and Regev A (2016). Div-Seq: Single-nucleus RNA-Seq reveals dynamics of rare adult newborn neurons. Science (New York, NY 353, 925–928.

Hafemeister C, and Satija R (2019). Normalization and variance stabilization of single-cell RNA-seq data using regularized negative binomial regression. Genome biology 20, 296. [PubMed: 31870423]

Hesketh PJ (2008). Chemotherapy-induced nausea and vomiting. N Engl J Med 358, 2482–2494. [PubMed: 18525044]

Horn CC (2009). Brain Fos expression induced by the chemotherapy agent cisplatin in the rat is partially dependent on an intact abdominal vagus. Auton Neurosci 148, 76–82. [PubMed: 19362521]

Hornby PJ (2001). Central neurocircuitry associated with emesis. Am J Med 111 Suppl 8A, 106S–112S. [PubMed: 11749934]

Hsu JY, Crawley S, Chen M, Ayupova DA, Lindhout DA, Higbee J, Kutach A, Joo W, Gao Z, Fu D, et al. (2017). Non-homeostatic body weight regulation through a brainstem-restricted receptor for GDF15. Nature 550, 255–259. [PubMed: 28953886]

Kawatani M, Yamada Y, and Kawatani M (2018). Glucagon-like peptide-1 (GLP-1) action in the mouse area postrema neurons. Peptides 107, 68–74. [PubMed: 30081042]

Krashes MJ, Koda S, Ye C, Rogan SC, Adams AC, Cusher DS, Maratos-Flier E, Roth BL, and Lowell BB (2011). Rapid, reversible activation of AgRP neurons drives feeding behavior in mice. J Clin Invest 121, 1424–1428. [PubMed: 21364278]

Lein ES, Hawrylycz MJ, Ao N, Ayres M, Bensinger A, Bernard A, Boe AF, Boguski MS, Brockway KS, Byrnes EJ, et al. (2007). Genome-wide atlas of gene expression in the adult mouse brain. Nature 445, 168–176. [PubMed: 17151600]

Lin HY, Harris TL, Flannery MS, Aruffo A, Kaji EH, Gorn A, Kolakowski LF Jr., Lodish HF, and Goldring SR (1991). Expression cloning of an adenylate cyclase-coupled calcitonin receptor. Science (New York, NY 254, 1022–1024.

Lindberg JS, Culleton B, Wong G, Borah MF, Clark RV, Shapiro WB, Roger SD, Husserl FE, Klassen PS, Guo MD, et al. (2005). Cinacalcet HCl, an oral calcimimetic agent for the treatment of secondary hyperparathyroidism in hemodialysis and peritoneal dialysis: a randomized, double-blind, multicenter study. J Am Soc Nephrol 16, 800–807. [PubMed: 15689407]

Luan HH, Wang A, Hilliard BK, Carvalho F, Rosen CE, Ahasic AM, Herzog EL, Kang I, Pisani MA, Yu S, et al. (2019). GDF15 Is an Inflammation-Induced Central Mediator of Tissue Tolerance. Cell 178, 1231–1244 e1211. [PubMed: 31402172]

Miller AD, and Leslie RA (1994). The area postrema and vomiting. Front Neuroendocrinol 15, 301–320. [PubMed: 7895890]

Mullican SE, Lin-Schmidt X, Chin CN, Chavez JA, Furman JL, Armstrong AA, Beck SC, South VJ, Dinh TQ, Cash-Mason TD, et al. (2017). GFRAL is the receptor for GDF15 and the ligand promotes weight loss in mice and nonhuman primates. Nat Med 23, 1150–1157. [PubMed: 28846097]

Oh SW, Harris JA, Ng L, Winslow B, Cain N, Mihalas S, Wang Q, Lau C, Kuan L, Henry AM, et al. (2014). A mesoscale connectome of the mouse brain. Nature 508, 207–214. [PubMed: 24695228]

Palmiter RD (2018). The Parabrachial Nucleus: CGRP Neurons Function as a General Alarm. Trends in neurosciences 41, 280–293. [PubMed: 29703377]

Pan W, Adams JM, Allison MB, Patterson C, Flak JN, Jones J, Strohbehn G, Trevaskis J, Rhodes CJ, Olson DP, et al. (2018). Essential Role for Hypothalamic Calcitonin ReceptorExpressing Neurons in the Control of Food Intake by Leptin. Endocrinology 159, 1860–1872. [PubMed: 29522093]

Parekh S, Ziegenhain C, Vieth B, Enard W, and Hellmann I (2018). zUMIs - A fast and flexible pipeline to process RNA sequencing data with UMIs. Gigascience 7.

Patel S, Alvarez-Guaita A, Melvin A, Rimmington D, Dattilo A, Miedzybrodzka EL, Cimino I, Maurin AC, Roberts GP, Meek CL, et al. (2019). GDF15 Provides an Endocrine Signal of Nutritional Stress in Mice and Humans. Cell Metab 29, 707–718 e708. [PubMed: 30639358]

Prescott SL, Umans BD, Williams EK, Brust RD, and Liberles SD (2020). An Airway Protection Program Revealed by Sweeping Genetic Control of Vagal Afferents. Cell 181, 574–589 e514. [PubMed: 32259485]

Price CJ, Hoyda TD, and Ferguson AV (2008). The area postrema: a brain monitor and integrator of systemic autonomic state. Neuroscientist 14, 182–194. [PubMed: 18079557]

Riediger T, Schmid HA, Lutz T, and Simon E (2001). Amylin potently activates AP neurons possibly via formation of the excitatory second messenger cGMP. Am J Physiol Regul Integr Comp Physiol 281, R1833–1843. [PubMed: 11705768]

Ritter S, McGlone JJ, and Kelley KW (1980). Absence of lithium-induced taste aversion after area postrema lesion. Brain research 201, 501–506. [PubMed: 7417860]

Satija R, Farrell JA, Gennert D, Schier AF, and Regev A (2015). Spatial reconstruction of single-cell gene expression data. Nature biotechnology 33, 495–502.

Schindelin J, Arganda-Carreras I, Frise E, Kaynig V, Longair M, Pietzsch T, Preibisch S, Rueden C, Saalfeld S, Schmid B, et al. (2012). Fiji: an open-source platform for biological-image analysis. Nature methods 9, 676–682. [PubMed: 22743772]

Secher A, Jelsing J, Baquero AF, Hecksher-Sorensen J, Cowley MA, Dalboge LS, Hansen G, Grove KL, Pyke C, Raun K, et al. (2014). The arcuate nucleus mediates GLP-1 receptor agonist liraglutide-dependent weight loss. J Clin Invest 124, 4473–4488. [PubMed: 25202980]

Sisley S, Gutierrez-Aguilar R, Scott M, D'Alessio DA, Sandoval DA, and Seeley RJ (2014). Neuronal GLP1R mediates liraglutide's anorectic but not glucose-lowering effect. J Clin Invest 124, 2456–2463. [PubMed: 24762441]

Slotnick B (2009). A simple 2-transistor touch or lick detector circuit. J Exp Anal Behav 91, 253–255. [PubMed: 19794837]

Tewson PH, Martinka S, Shaner NC, Hughes TE, and Quinn AM (2016). New DAG and cAMP Sensors Optimized for Live-Cell Assays in Automated Laboratories. J Biomol Screen 21, 298–305. [PubMed: 26657040]

Tfelt-Hansen J, and Brown EM (2005). The calcium-sensing receptor in normal physiology and pathophysiology: a review. Crit Rev Clin Lab Sci 42, 35–70. [PubMed: 15697170]

Thorens B (1992). Expression cloning of the pancreatic beta cell receptor for the gluco-incretin hormone glucagon-like peptide 1. Proceedings of the National Academy of Sciences of the United States of America 89, 8641–8645. [PubMed: 1326760]

Tsai VWW, Husaini Y, Sainsbury A, Brown DA, and Breit SN (2018). The MIC-1/GDF15-GFRAL Pathway in Energy Homeostasis: Implications for Obesity, Cachexia, and Other Associated Diseases. Cell Metab 28, 353–368. [PubMed: 30184485]

Vong L, Ye C, Yang Z, Choi B, Chua S Jr., and Lowell BB (2011). Leptin action on GABAergic neurons prevents obesity and reduces inhibitory tone to POMC neurons. Neuron 71, 142–154. [PubMed: 21745644]

Williams EK, Chang RB, Strochlic DE, Umans BD, Lowell BB, and Liberles SD (2016). Sensory Neurons that Detect Stretch and Nutrients in the Digestive System. Cell 166, 209–221. [PubMed: 27238020]

Yamamoto H, Kishi T, Lee CE, Choi BJ, Fang H, Hollenberg AN, Drucker DJ, and Elmquist JK (2003). Glucagon-like peptide-1-responsive catecholamine neurons in the area postrema link peripheral glucagon-like peptide-1 with central autonomic control sites. J Neurosci 23, 2939–2946. [PubMed: 12684481]

Yang L, Chang CC, Sun Z, Madsen D, Zhu H, Padkjaer SB, Wu X, Huang T, Hultman K, Paulsen SJ, et al. (2017). GFRAL is the receptor for GDF15 and is required for the anti-obesity effects of the ligand. Nat Med 23, 1158–1166. [PubMed: 28846099]

Zilionis R, Nainys J, Veres A, Savova V, Zemmour D, Klein AM, and Mazutis L (2017). Single-cell barcoding and sequencing using droplet microfluidics. Nat Protoc 12, 44–73. [PubMed: 27929523]

Zuger D, Forster K, Lutz TA, and Riediger T (2013). Amylin and GLP-1 target different populations of area postrema neurons that are both modulated by nutrient stimuli. Physiology & behavior 112-113, 61–69. [PubMed: 23438370]

Highlights

- Single-nucleus RNAseq provides an atlas of area postrema neurons and receptors.
- Genetic tools reveal neurons and receptors that evoke nausea-like behaviors in mice.
- Behavioral responses to poisons are lost after cell ablation or gene knockout.
- Certain excitatory neuron subtypes project to PBN alarm neurons containing CGRP.

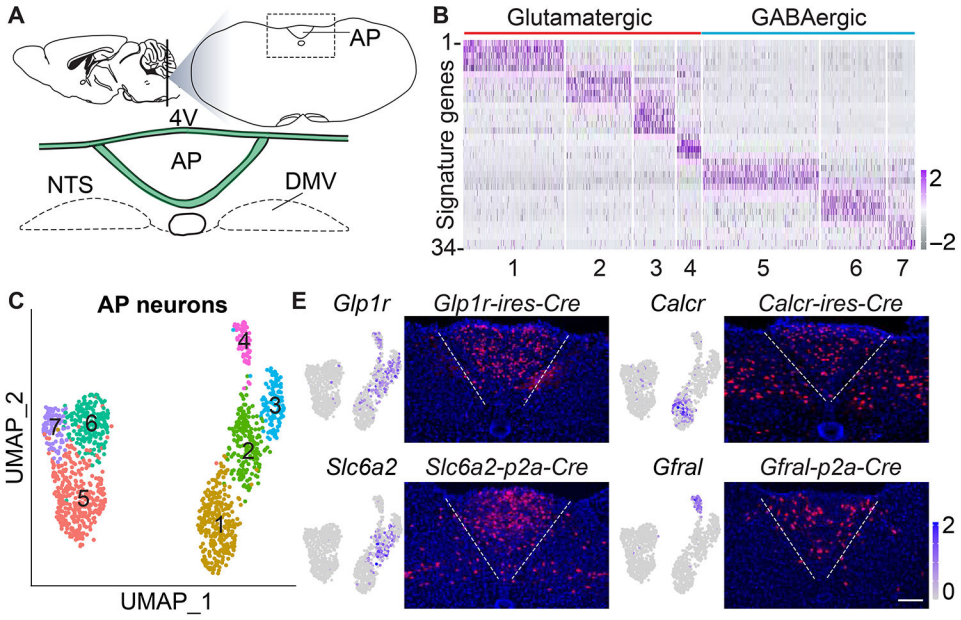

D

Cluster	1	2	3	4	5	6	7
Cre line	*Calcr*	*Slc6a2*	-	*Gfral*	-	-	-
Surface receptor genes	*Olfr78* *Calcr* *Lifr* *Tacr3* *Bdkrb2* *Tmem163* *Tmem178* *Fgfr1* *Trpc3*	*Casr* *Paqr8* *Tmem35a* *Cd24a* *Npy1r* *Glp1r*	*Agtr1a* *Prlhr* *Glp1r* *Gpr149* *Ghr* *Ntrk3* *Sorcs1*	*Gpr88* *Gfral* *Trpm3* *Glp1r* *Casr* *Erbb4*	*Gpr83* *Ptprk* *Epha6* *Hcn1* *Ptprt* *Ephb6*	*Gipr* *Adgrl2* *Tmem132d* *Unc5d* *Tmem158*	*Ntrk1* *Gpr139* *Tmem215* *Vldlr* *Tmem132d*
Neuro-transmitter related genes	*Slc17a6* *Gal*	*Slc17a6* *Th* *Ddc* *Dbh*	*Slc17a6* *Ddc* *Dbh*	*Slc17a6* *Cck* *Nts* *Ddc*	*Gad2*	*Gad2* *Penk* *Nppc*	*Gad2* *Sst*

Figure 1. Genetic control over an area postrema cell atlas

(A) Cartoon indicating area postrema (AP) location in the brainstem; 4V: fourth ventricle; AP: area postrema; DMV: dorsal motor nucleus of the vagus. (B) Normalized expression levels of 34 cluster-defining signature genes (see Table S1 for gene names) across all cells from clusters 1-7. (C) Uniform manifold approximation and projection (UMAP) plots based on single-cell transcriptome data showing seven area postrema neuron types (color coded) including excitatory (clusters 1-4) and inhibitory neurons (clusters 5-7). (D) Receptor and neurotransmitter-related genes expressed in area postrema neuron types. (E) UMAP plots indicating expression of Cre-targeted genes in area postrema neurons (left). Cre lines indicated were crossed to a *Rosa26-LSL-tdTomato* reporter, and native fluorescence visualized in coronal area postrema cryosections (right), scale bars: 100 μm. See also Figure S1, S2 and Table S1.

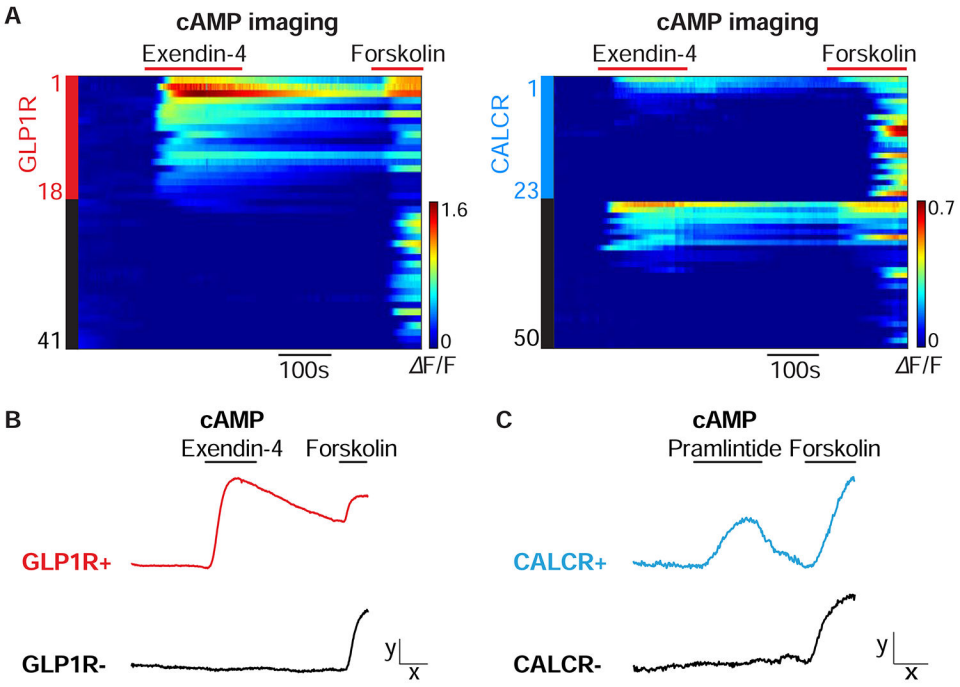

Figure 2. Imaging responses of area postrema neurons

(A) Area postrema neurons of *Glp1r-ires-Cre; Rosa26-LSL-tdTomato* (left) or *Calcr-ires-Cre; Rosa26-LSL-tdTomato* (right) mice were acutely dissociated and transfected with the cAMP sensor cADDis. Rows indicate responses (Δ*F/F*, color scale) of individual neurons over time, with exendin-4 (100 nM) and forskolin (25 μm) applied at times indicated (red bars). Y-axis colored bars (left: red; right: blue) and black bars indicated tdTomato-positive and tdTomato-negative neurons respectively. (B, C) Area postrema neurons were harvested from *Glp1r-ires-Cre; Rosa26-LSL-tdTomato* (B) or *Calcr-ires-Cre; Rosa26-LSL-tdTomato* mice (C) for transfection-based cAMP imaging. Representative responses of GLP1R-positive (red), CALCR-positive (blue), and reporter-negative (black) neurons are shown to exendin-4 (100 nM), pramlintide (100 nM), and forskolin (25 μM) x: 100 seconds, y: 0.5 Δ*F/F*.

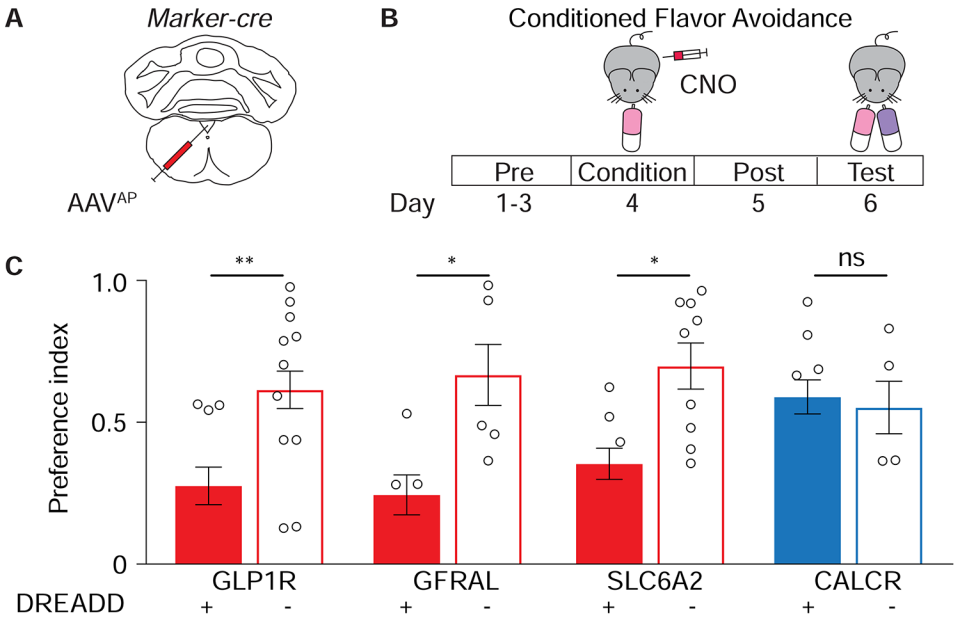

Figure 3. Multiple area postrema neuron types promote flavor avoidance

(A) Cartoon of AAV infection in area postrema. (B) Timeline of behavioral assay for conditioned flavor avoidance. (C) *Glp1r-ires-Cre* (GLP1R), *Gfral-p2a-Cre* (GFRAL), *Slc6a2-p2a-Cre* (SLC6A2), and *Calcr-ires-Cre* (CALCR) mice were injected with AAVs encoding Cre-dependent $G\alpha_s$-DREADD-mCherry (+) or tdTomato (−), and analyzed for CNO-evoked flavor avoidance. (n=5-15, mean ± sem, circles: individual data points, *p<.05, **p<.01. See also Figure S3, S4.

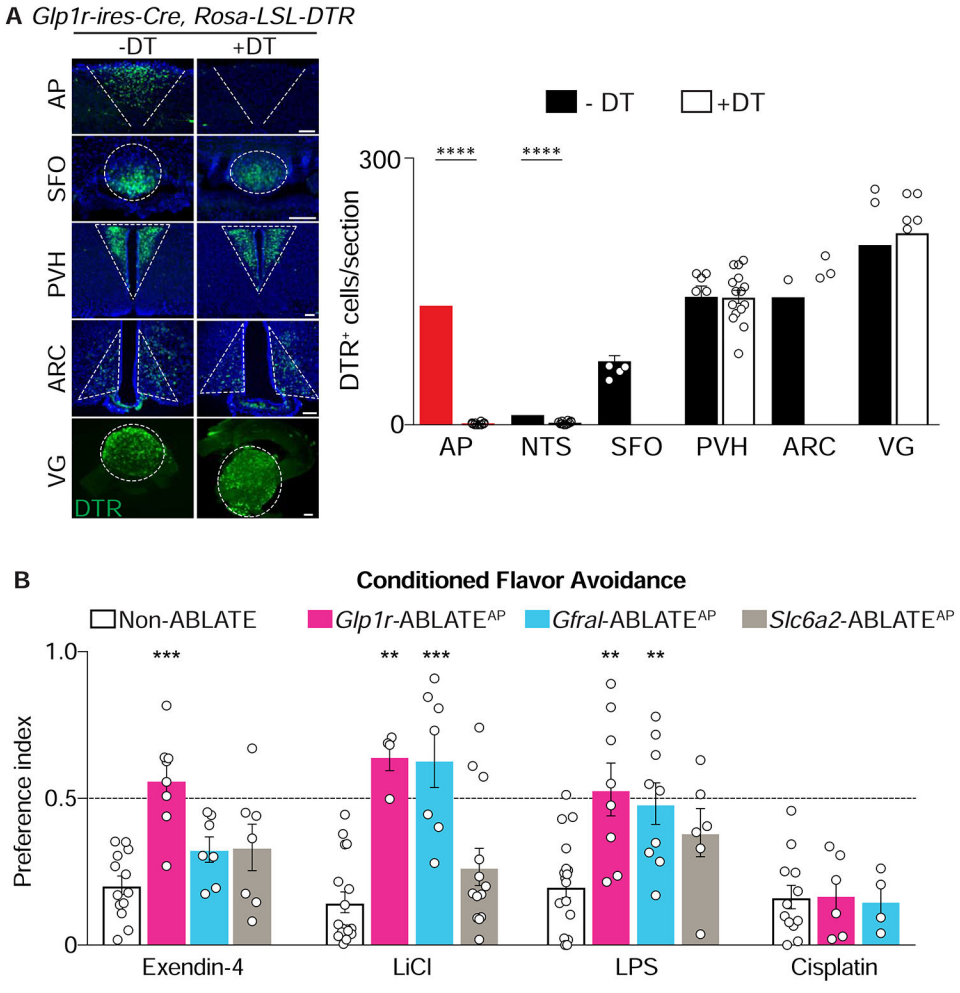

Figure 4. Neuron ablation eliminates behavioral responses to visceral poisons

(A) The area postrema of *Glp1r-ires-Cre; Rosa26-LSL-DTR* mice was injected with DT (+DT) or saline (−DT). Immunohistochemistry for DTR (left) and quantification of DTR-expressing cells (right) in coronal brain cryosections containing area postrema (AP), subfornical organ (SFO), paraventricular hypothalamus (PVH), and arcuate nucleus (ARC) or in wholemounts of vagal ganglia (VG), scale bar: 100 μm, n=4-21 sections from 4 mice (−DT) or 14 mice (+DT), mean ± sem, circles: individual data points, ****p<.0001. (B) The ability of exendin-4, lithium chloride (LiCl), lipopolysaccharide (LPS), and cisplatin to condition flavor avoidance in Non-ABLATE, *Glp1r*-ABLATE^{AP}, *Slc6a2*-ABLATE^{AP}, and *Gfral*-ABLATE^{AP} mice, n=4-18, mean ± sem, circles: individual data points, **p<.01, ***p<.001, statistical comparisons to non-ABLATE mice. See also Figure S5.

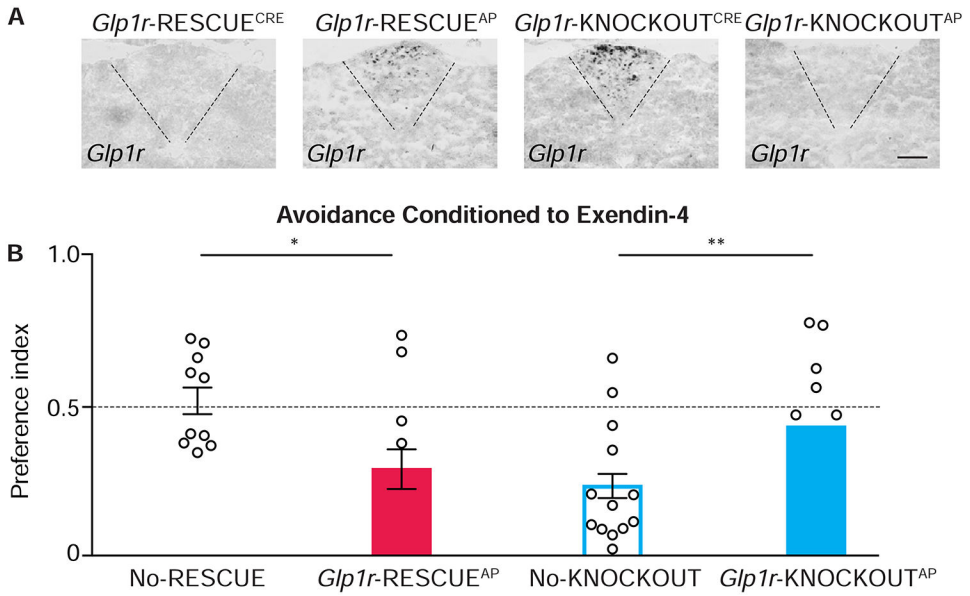

Figure 5. Cell-specific knockout and rescue of *Glp1r* impacts flavor avoidance

(A) *In situ* hybridization to detect *Glp1r* mRNA in coronal area postrema cryosections from mice indicated, scale bar: 100 μm. (B) The ability of exendin-4 to condition flavor avoidance was measured in mice indicated, n=11-18, mean ± sem, circles: individual data points, *p<.05, **p<.01. See also Figure S5.

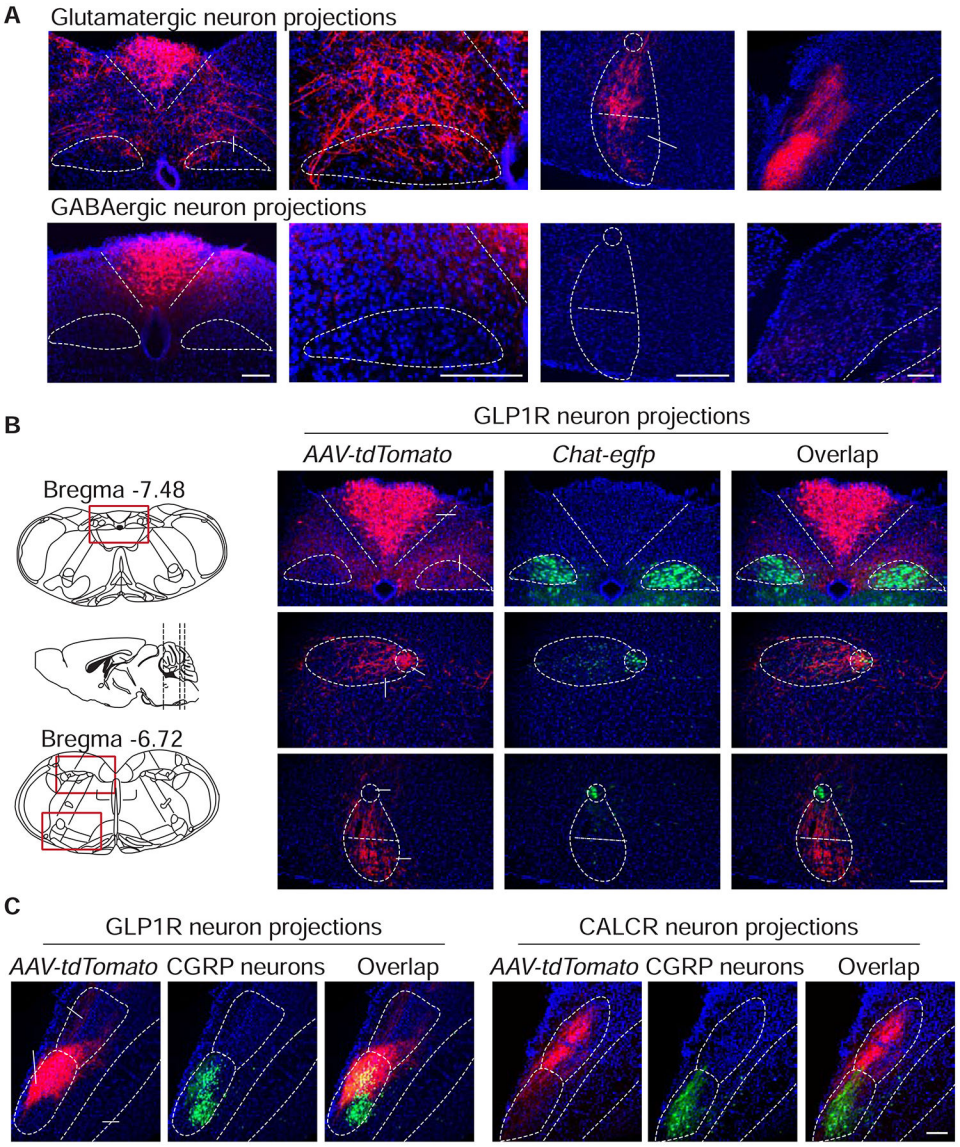

Figure 6. Cell-type specific projections of area postrema neurons

(A) *AAV-Flex-tdTomato* was injected into the area postrema of *Slc17a6-ires-Cre* (top) and *Gad2-ires-Cre* (bottom) mice, and tdTomato-positive fibers were visualized by immunohistochemistry. (B) *AAV-Flex-tdTomato* was injected into the area postrema of *Glp1r-ires-Cre*; *Chat-gfp* mice. GFP was visualized by native fluorescence and tdTomato-positive fibers were visualized by immunohistochemistry. (C) *AAV-Flex-tdTomato* was injected into the area postrema of *Glp1r-ires-Cre*; *Calca-gfp* and *Calcr-ires-Cre*; *Calca-gfp* mice. GFP was visualized by native fluorescence (CGRP neurons) and tdTomato-positive fibers were visualized by immunohistochemistry, AP: area postrema; DMV: dorsal motor nucleus of the vagus; Amb: nucleus ambiguus; RVLM: rostral ventrolateral medulla; PBN: parabrachial nucleus; dl: dorsolateral; el: external lateral; scp: superior cerebellar peduncle; scale bars: 100 μm. See also Figure S6, S7.

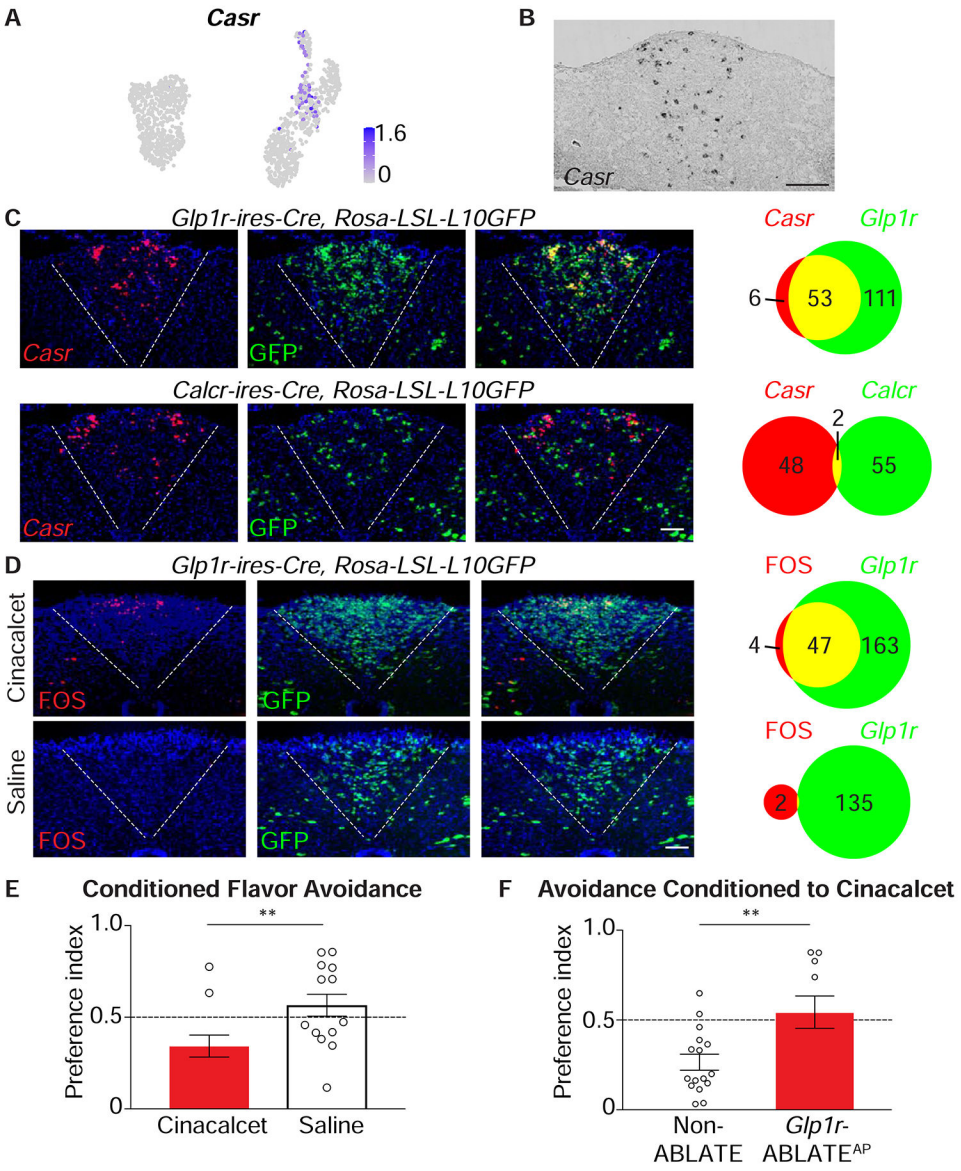

Figure 7. A neural basis for behavioral aversion conditioned by cinacalcet

(A) UMAP plot depicting *Casr* expression across area postrema neurons. (B) *In situ* hybridization to detect *Casr* mRNA in coronal area postrema cryosections, scale bar: 100 μm. (C) Two-color expression analysis showing *in situ* hybridization to detect *Casr* mRNA (red) and native GFP fluorescence (green) in coronal area postrema cryosections of *Glp1r-ires-Cre; Rosa26-LSL-L10GFP* and *Calcr-ires-Cre; Rosa26-LSL-L10GFP* mice, scale bar: 100 μm. The numbers of co-labeled (yellow) or individually labeled (red, green) cells were counted (right). (D) Fos immunohistochemistry (red) and native GFP fluorescence (green) were analyzed in coronal area postrema cryosections after intraperitoneal injection of cinacalcet or saline alone in *Glp1r-ires-Cre; Rosa26-LSL-L10GFP* mice, scale bar: 100 μm. (E) The ability of intraperitoneal cinacalcet or saline to condition flavor avoidance was measured in wild-type mice, n=11-14, mean ± sem, circles: individual data points, **p<.01.

(F) The ability of cinacalcet to condition flavor avoidance was measured in Non-ABLATE and *Glp1r*-ABLATE^{AP} mice, n=10-16, mean ± sem, circles: individual data points, **p<.01.

KEY RESOURCES TABLE

REAGENT or RESOURCE	SOURCE	IDENTIFIER
Antibodies		
Rabbit-anti-RFP	Rockland	Cat# 600-401-379; RRID:AB_2209751
Goat-anti-HB-EGF (anti-DTR)	R&D Systems	Cat# AF-259-NA, RRID:AB_354429
Rabbit-anti-Fos	Synaptic Systems	Cat# 226 003, RRID:AB_2231974
Sheep-anti-GFR alpha-like antibody	R&D Systems	Cat# AF5728, RRID:AB_2110592
Anti-Digoxigenin-AP, Fab fragments	Roche	Cat# 11093274910, RRID:AB_514497
Bacterial and Virus Strains		
AAV9-CAG-Flex-tdTomato	Oh et al., 2014	Addgene, Cat #51503-AAV9
AAV9-Ef1a-DIO-hChR2(H134R)-mCherry	Gift from Karl Deisseroth	Addgene, Cat #20297-AAV9
pAAV-hSyn-DIO-rM3D (Gα$_s$)-mCherry	Gift from Bryan Roth	Addgene, Cat #50458
pAAV-hSyn-DIO-hM3D(Gα$_q$)-mCherry	Krashes et al., 2011	Addgene, Cat #44361
AAV9-Ef1a-DIO-EYFP	Gift from Karl Deisseroth	Addgene, Cat #27056-AAV9
AAV1-CAG-Cre-mCherry	SignaGen	SignaGen, Cat #SL101117
AAV1-CAG-mCherry	SignaGen	SignaGen, Cat #SL101127
AAVrg-Flex-tdTomato	Gift from Edward Boyden	Addgene, Cat #28306-AAVrg
AAVrg-hSyn-DIO-GFP	Gift from Bryan Roth	Addgene, Cat #50457-AAVrg
Green Up cADDis cAMP sensor	Montana Molecular	Cat # U0200G
Chemicals, Peptides, and Recombinant Proteins		
Exendin-4	Tocris	Cat #1933
Clozapine N-oxide dihydrochloride	Tocris	Cat #6329
Cisplatin	Tocris	Cat #2251
Cinacalcet hydrochloride	Tocris	Cat #6170
Forskolin	Tocris	Cat #1099
Pramlintide	Tocris	Cat #5031
Lipopolysaccharide, *Salmonella typhimurium*	Sigma-Aldrich	Cat #437650
Diphtheria Toxin from *Corynebacterium diphtheriae*	Sigma-Aldrich	Cat #D0564
IGEPAL-CA-630	Sigma-Aldrich	Cat #I8896
6,7-dinitroquinoxaline-2,3-dione	Sigma-Aldrich	Cat #D0540
DL-AP5	Tocris	Cat #0105
Tetrodotoxin	Tocris	Cat #1078
FluoroGold	Santa Cruz Biotechnology	Cat #sc-358883
Critical Commercial Assays		
Papain dissociation system	Worthington Biochemical	Cat # LK003150
TSA-Cy5.5	Perkin-Elmer	Cat # NEL766001KT
MegaScript T7 kit	Invitrogen	Cat # AM1334
Deposited Data		

REAGENT or RESOURCE	SOURCE	IDENTIFIER
Raw images	This study	Mendeley data: doi:10.17632/tpw4c3g9m3.1
Single-nucleus sequencing	This study	GEO accession number: GSE160938
Single-nucleus sequencing analysis	This study	GitHub:http://github.com/jakaye/AP_scRNA
Experimental Models: Organisms/Strains		
Glp1r-ires-Cre	Chang et al., 2015; Williams et al.,2016	Deposited in Jackson laboratory (Cat#029282)
Slc17a6-ires-Cre (Vglut2)	Vong et al., 2011	N/A
Calcr-ires-Cre	Pan et al., 2018	N/A
Glp1r-KNOCKOUT^{Cre}	Sisley et al., 2014	N/A
Glp1r-RESCUE^{Cre}	Unpublished, gift from Randy Seeley (University of Michigan)	N/A
Calca-gfp	GENSAT	RRID:MMRRC_011187-UCD
Wild-type C57BL/6J	Jackson Laboratory	Cat #000664
Rosa-LSL-L10GFP	Jackson Laboratory	Cat #024750
Chat-gfp	Jackson Laboratory	Cat #007902
Rosa-LSL-tdTomato	Jackson Laboratory	Cat #007908
Gad2-ires-Cre	Jackson Laboratory	Cat #010802
Rosa-LSL-DTR	Jackson Laboratory	Cat #007900
Slc6a2-p2a-Cre	This study	N/A
Gfral-p2a-Cre	This study	N/A
Software and Algorithms		
MATLAB R2019a	MathWorks	RRID: SCR_001622 https://www.mathworks.com/products/matlab.html
The R Project for Statistical Computing	R Core Team, 2019	https://www.R-project.org/
Seurat v3.1.5	Butler et al., 2018; Satija et al., 2015	https://satijalab.org/seurat/
PRISM 7	GraphPad	RRID: SCR_002798 https://www.graphpad.com/scientific-software/prism/
FIJI	Schindelin et al., 2012	RRID:SCR_002285 https://fiji.sc
BioRender	BioRender.com	RRID:SCR_018361 https://biorender.com